Eco-Friendly Controlled-Release Nano-Biofertilizer Combining Silver Nanoparticles and *Azospirillum* Enhances Tomato Growth and Nitrogen Use Efficiency.

Abstract

Over-reliance on chemical N fertilizers has significantly increased crop production but has also led to extremely low nitrogen use efficiency (NUE) and serious environmental issues. In this investigation, a biodegradable nanobiofertilizer, PS+[AZO+G-AgNPs] was prepared using green-synthesized silver nanoparticles (AgNPs) from *Allium sativum* leaf extract, incorporating *Azospirillum spp*., immobilized in a porous starch (PS) matrix and hydrogel bead system. Physicochemical characterization confirmed the synthesis of stable, crystalline AgNPs (~100 nm) with good colloidal stability, as well as successful microbial conjugation. An experimental station was conducted on tomatoes under 100%, 50%, and 25% of the recommended nitrogen dose (RDN). Two-way ANOVA showed that treatments, nitrogen gradients, and the interaction between treatments and nitrogen all had significant effects on biomass accumulation, nutrient absorption, yields, and fruit quality. The nitrogen uptake efficiency, dry matter accumulation, total yield, and fruit weight were significantly increased by PS+[Azo+AgNPs], especially at 50–100% RDN. Increases in vitamin C, firmness, and total soluble solids are associated with enhanced carbon–nitrogen metabolism and antioxidant capacity. The results show that the proposed nanobiointegrated platform synchronizes nutrient inputs, reduces nitrogen dependence, and increases yield and fruit quality. This biodegradable system provides an environmentally friendly approach to improve NUE and reduce the environmental pollution associated with traditional fertilization.

Key words: Silver nanoparticles; porous starch; targeted delivery; quality; nitrogen use efficiency; *Azospirillum* ; nanofertilizer; eco-friendly

Introduction

The food production system has become intensified globally to feed an increasing population, and reliance on synthetic nitrogen (N) fertilizers has reached unprecedented levels. While nitrogen fertilizers have significantly increased crop production, their nutrient use efficiency (NUE) is still appallingly low, with estimates that crop plants actually utilize less than 50% of applied nitrogen. The remaining one-third is lost as nitrogen (N) emissions, such as nitrate leaching, ammonia volatilization [1], and denitrification, causing groundwater contamination, eutrophication [2], soil acidification, and nitrous oxide (N_2O: a potent greenhouse gas) emission. The importance of enhancing NUE for sustainable agricultural intensification and climate change mitigation has been highlighted by recent evaluations [3-5].

Controlled-release fertilizers (CRFs) have been developed as a potential technological solution to combat these problems. CRFs synchronize nutrient release with crop uptake, thereby improving N retention in the rhizosphere, reducing environmental losses, and enhancing agronomic utilization efficiency. Recent innovations focus on incorporating degradable polymers and bio-based matrices to address microplastic residues from traditional polymer-coated fertilizers [6-9].In this respect, starch-based porous carriers have received considerable attention, as they are renewable, biodegradable, low-cost materials with customizable release kinetics.

Concurrently, biofertilizers (particularly PGPR) are gaining attention as integral parts of sustainable soil fertility management strategies. Nitrogen-fixing microorganisms have been used, such as strains of *Azospirillum spp*. improve the rhizobium-independent synthesis pathway and root system; increase cytokinin synthesis and reduce ethylene production. Shedding during the growth of reproductive organs, but this can meet the baby's needs for high-yield selection. Recent research showed that combining PGPR with various advanced carrier systems greatly enhanced its survival in microbial cells and field performance [10-11]. Next-generation fertilizers could be leveraged to a great extent by nanotechnology, such as nanoencapsulation, improved surface interactions, targeted nutrient release, and enhanced stability. Green-synthesized silver nanoparticles (AgNPs), especially those prepared using plant extracts, exhibit antimicrobial activity, biocompatibility, and improved plant physiological responses, depending on the applied concentration. Green synthesis methods using Allium sativum extracts are considered environmentally friendly, inexpensive, and scalable alternatives to traditional chemical syntheses [12-13].

Although advances have been made in CRFs, biofertilizers, and nanomaterials independently, few studies have examined their combined use to form an integrated biodegradable nanobiofertilizer platform. This work specifically reports a new bio-based AgNP formulation comprising green-synthesized AgNPs from *Allium sativum* leaf extract and *Azospirillum*, immobilized in biodegradable porous starch (PS) matrices. The use of natural polymeric carriers is intended to provide controlled nutrient release, improved microbial viability, enhanced rhizosphere interactions, and reduced synthetic nitrogen use.

The PS+[Azo+A-AgNPs] nano-biofertilizer would promote nitrogen uptake efficiency, improve plant growth and fruit yield, and enhance fruit quality in tomato (*Solanum lycopersicum L.*) at lower rates of nitrogen inputs. Accordingly, in this work, we test the agronomic performance, nitrogen use efficiency, fruit yield, and quality parameters of a novel nanobiofertilizer under controlled greenhouse conditions to orient the development of environmentally friendly fertilization strategies.

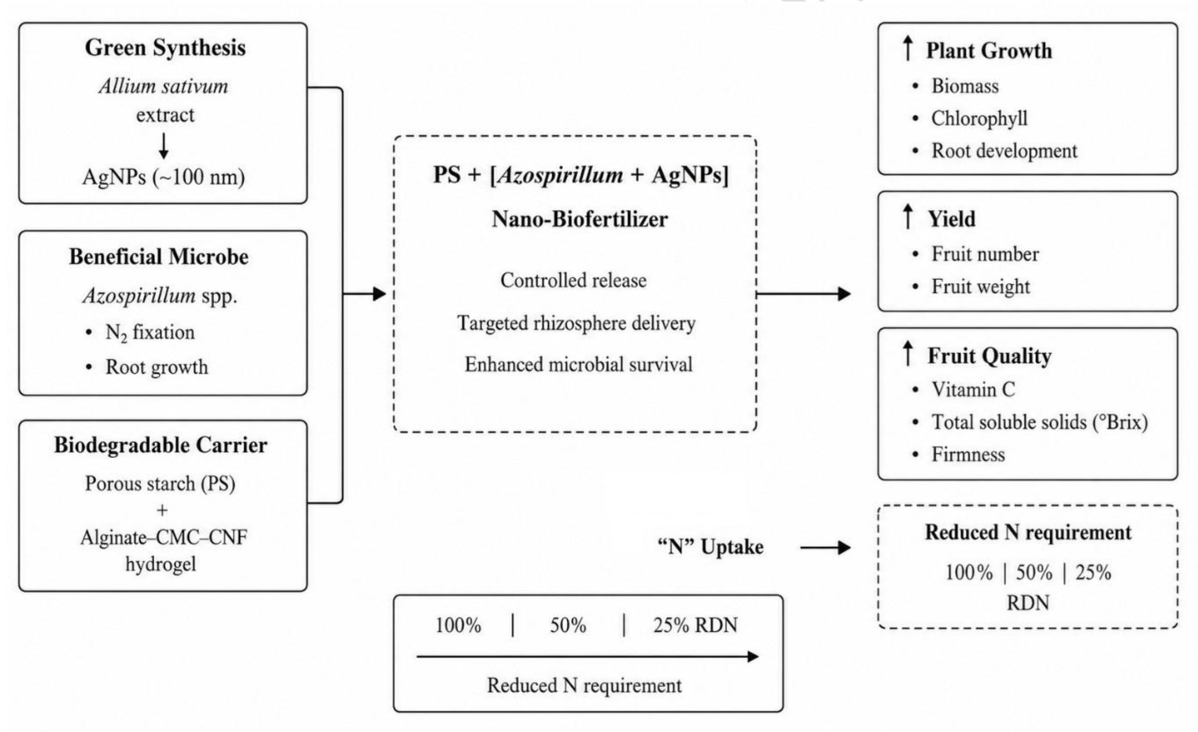

Figure 1. Conceptual framework of the eco-friendly controlled-release PS+[AZO+G-AgNPs] nano-biofertilizer system.

Materials and Methods

2.1 Chemicals and Biological Materials

Silver nitrate ($AgNO_3$, purity ≥99.9%) was purchased from Merck Life Science Pvt. Ltd. (Mumbai, India). Sodium alginate (medium viscosity), carboxymethyl chitosan (CMC, degree of deacetylation ≥85%), and cellulose nanofibers (CNF) were purchased from Sigma-Aldrich (India). Food-grade, high-amylose-content porous starch was obtained from a certified supplier and used as a biodegradable carrier matrix with no further modification.

A commercial suspension of *Azospirillum* spp. (minimum viable count $\geq 10^8$ CFU g^{-1}) was purchased from a registered local agricultural bio-input supplier and kept at 4°C until in use. Healthy, disease-free leaves of *A. sativum L.* were amassed from an organic garden, washed with distilled water, and shade-dried before being subjected to extraction. All reagents were analytical reagents, and ultrapure distilled water was used in all experiments.

2.2 Green synthesis of silver nanoparticles (A-AgNPs)

Aqueous leaf extract of *A. sativum* was extracted by boiling 10 g of crushed fresh leaves in distilled water (100 mL) at 80°C for 20 min and filtering through Whatman No. 1 filter paper. For the synthesis of nanoparticles, 10 mL of leaf extract was slowly added to 90 mL of a 1 mM $AgNO_3$ solution under continuous magnetic stirring at 80 °C for 3 h. The generation of A-AgNPs was initially evident from the visual observation of a color change from pale yellow to dark brown, resulting from surface plasmon resonance (SPR) [14-16].

The suspension was centrifuged at 15,000 × g for 1 h at 4°C, and the pellet was washed three times with distilled water to desorb unreacted biomolecules, followed by freeze-drying. The dry nanoparticles were stored in amber glass vials at 4 °C until use.

2.3 Synthesis of A-AgNPs–Azospirillum Conjugate (A-AgNPs–Azo)

$AgNO_3$ solution was prepared in Milli-Q water, and a sufficient volume (1%) was added to the *Azospirillum* culture in BFS medium for the reduction process. A-AgNPs were resuspended in sterile distilled water (5 µg mL^{-1}) after a mild ultrasonication. The suspension was magnetically stirred for 10 min under aseptic conditions to permit surface adsorption and interaction, and an equal volume of *Azospirillum* suspension (adjusted to ~10^8 CFU mL^{-1}) was added [17].

The centrifuged conjugate blend was subjected to a 15-min spin at 12,000 × g. The supernatant was harvested to enumerate non-adherent bacterial cells. The encapsulation/loading efficiency (LE%) was derived from the following equations:

$$LE(\%) = \frac{W_i - W_f}{W_i} \times 100$$

where Wi is the initial bacterial concentration, and Wf is the free bacterial concentration in the supernatant.

2.4. Porous Starch (PS) Matrix

Porous Starch (PS) Matrix Encapsulation originated from traditional encapsulation in porous starch granule preparation method. A-AgNPs–Azo conjugate (10 mg mL^{-1} equivalent) was combined with porous starch powder according to a weight ratio of 1.5:1 (g mL^{-1}). This mixture was incubated at 37°C with shaking (150 rpm) for 12 h to adsorb or entrap the particles in the starch pores. The pellet was centrifuged at 8,000 × g for 10 minutes and oven-dried (at 40°C) to a constant weight. The dried formulation (PS+[Azo+A-AgNPs]) was kept in a sterilized, airtight vessel until bead formation [18].

2.5 Making of Composite Hydrogel Beads

The hydrogel beads were fabricated by sodium alginate (SA), carboxymethyl chitosan (CMC), and cellulose nanofibers (CNF). In a nutshell, a 2% (w/v) SA solution was prepared in deionized water, and then 1% (w/v) CMC and 0.5% (w/v) CNF were added with stirring. The polymeric blend was mixed with the PS+ [Azo+A-AgNPs] composite. Then mixture was vacuum-degassed to remove trapped air bubbles and extruded in small volumes using a sterile syringe into a 2% (w/v) $CaCl_2$ solution for ionic cross-linking. The beads were gelatinized for 30 min, washed with distilled water, and dried at room temperature.

3. Characterization

3.1 Physicochemical Characterization

UV–Visible Spectroscopy:

The surface plasmon resonance spectrum of A-AgNPs was monitored using a Shimadzu UV-1800 spectrophotometer over 300–700 nm.

Fourier Transform Infrared Spectroscopy (FTIR):

FTIR analyses (PerkinElmer, 1750) were performed in the 4000–1.99 µm range to examine functional groups and interactions among nanoparticles, bacterial cells, and polymer matrices.

Dynamic Light Scattering (DLS) and Zeta Potential:

Hydrodynamic sizes, PDI, and zeta potentials were measured using a Malvern Zetasizer Nano instrument at 25°C.

X-ray Diffraction (XRD):

The XRD pattern of AgNPs was analyzed on a Rigaku Ultima IV diffractometer (Cu Kα radiation (λ = 1.5406 Å)) in the 2θ range from 20 to 80°.

3.2 Greenhouse Experimental Design

Tomato (*Solanum lycopersicum* L.) seeds were sown in sterilized nursery trays, and 4-week-old transplants were transferred to plastic pots (10 kg) filled with a mixture of clay-loamy soil, pH 6.8 ± 0.2; organic carbon content: 0.75%. The experiment was conducted using a randomized complete block design (RCBD) with five fertilizer treatments and three levels of nitrogen (100, 50, and 25% RDN) in six replicates. Fertilizer was applied 15, 30, and 60 days after transplantation (DAT). The plants were grown in a greenhouse at 25 ± 2°C (day), 18 ± 2°C (night), with a relative humidity of 60–70% and a natural photoperiod.

3.3 Evaluation of Plant Growth, Yield, and Quality

At 15 days after full fertilization, vegetative parameters, including plant height, leaf number, branch number, and stem diameter, were evaluated, along with SPAD chlorophyll content. Fruit number per plant, individual fruit weight, fruit diameter, fruit length, and total yield per plant were recorded at the time of harvest. Quality characteristics, such as total soluble solids (°Brix), titratable acidity, and vitamin C content, were determined according to AOAC standard procedures. Nitrogen uptake was assayed by the Kjeldahl method, and nitrogen use efficiency (NUE) was determined as follows:

$$NUE = \frac{Yield_N - Yield_0}{N_{applied}}$$

3.4 Statistical Analysis

The data were subjected to a two-way ANOVA to test the influence of fertilizer treatments and N levels. Tukey's HSD test at $p < 0.05$ was used to compare means. Statistical analysis was performed using MSTAT Version 2.1 and SPSS. To visualize treatment interactions and response patterns, we constructed the heat map.

Table 1. Chemical and physical properties of soil used in the tomato pot experiment.

Parameter	Value
pH	7.34
Total Calcium Carbonate (TCC, %)	2.6
Organic Carbon (OC, %)	1.55
Available Nitrogen (N, mg/kg)	110.2
Available Phosphorus (P, mg/kg)	13.3
Available Potassium (K, mg/kg)	219

Coarse Sand (%)	4.4
Fine Sand (%)	30.0
Silt (%)	26.8
Clay (%)	36.9

4. Result and discussion

4.1 UV–visible absorption spectra

The successful phyto-mediated synthesis of silver nanoparticles using *Allium sativum* extract was established by UV–visible absorption spectra (Figure 2). The crude garlic extract showed a wide absorption band below 350 nm, which was due to π–π* transitions of phenolic and aromatic type phytoconstituents in the extract as observed in several plant-derived extracts (Kumar et al., 2022), and when reacted with $AgNO_3$, another band indicating a surface

plasmon resonance (SPR) at ~ 430 nm was also seen, confirming the reduction of Ag^+ ions to

metallic Ag^0 nanoparticles. The SPR maximum is within the characteristic 400–450 nm range found for spherical AgNPs smaller than 50 nm [3,19], indicating controlled nucleation and limited aggregation. After conjugation, slight peak broadening and a marginal red shift can be observed, indicating surface functionalization and minor dielectric changes. Also, fulfillment of SPR intensity suggests preservation of colloidal stability identical to that of nano-bio hybrid systems.

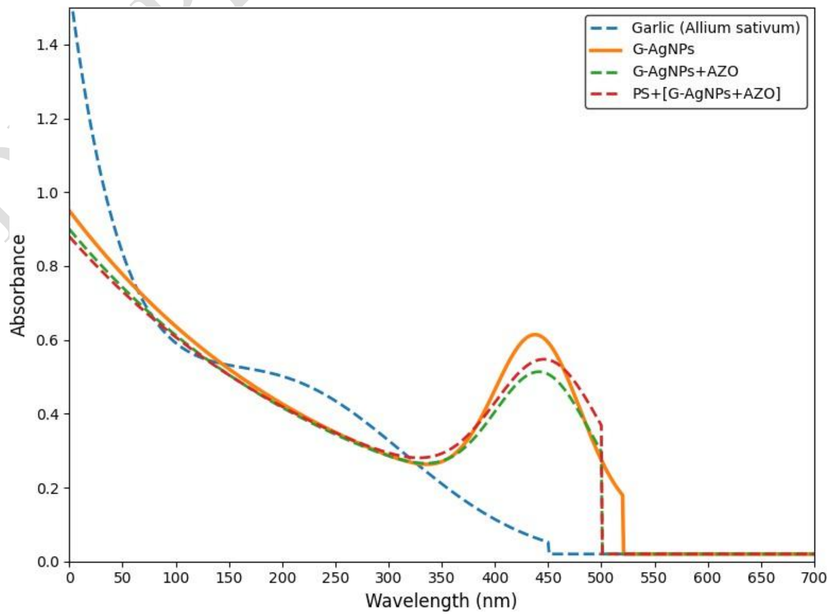

Figure 2 Biosynthesis of silver nanoparticles: UV spectra of the aqueous leaf extract and G-

AgNPs synthesized from the Garlic (*Allium sativum*) leaf extract

4.2 X-Ray Diffraction (XRD) Analysis

The X-ray diffraction pattern reveals four distinct diffraction peaks approximately located at 2θ ≈ 38°, 44°, 64°, and 77°, respectively, which can be readily assigned to the (111), (200), (220), and (311) crystallographic planes of face-centered cubic (fcc) in Figure 3,. The predominance of the (111) reflection indicates preferred orientation along the most thermodynamically stable plane, suggesting energetically favorable crystal growth during biosynthesis. For plant-mediated AgNPs synthesized via green pathways, similarly broad diffraction profiles have often been reported and display fcc crystalline structures independent of the botanical agent used [13,19].

The pronounced, sharp diffraction peaks obtained in the current investigation characterize a very high crystallinity and phase purity, comparable to those of polymer-stabilized or polysaccharide-encapsulated AgNPs reported by Kumar et al. (2022) and Li et al. (2023). Crucially, there were no significant peak shifts or new impurity phases upon AZO conjugation followed by porous starch (PS) encapsulation treatment, confirming retention of the metallic core structure. A similar structural stability following polymer embedding was reported for nanobio-composite fertilizers, in which the AgNPs' cores maintained their crystalline structure within biopolymeric shells [6,7]. Crystallinity is intrinsically important in the mechanistic context of silver ion release kinetics. This may lead to more orderly oxidative dissolution and more predictable Ag^{+} diffusion than in their amorphous counterparts, thereby enhancing functional robustness across soil microenvironments and sustainable agricultural systems .

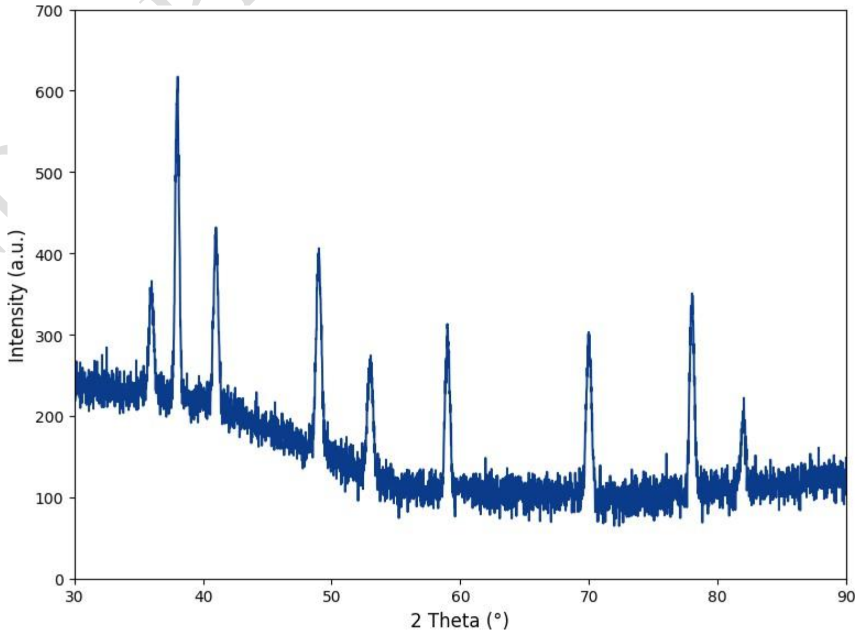

Figure 3. XRD pattern of the synthesized G-AgNPs using Garlic (*Allium sativum*) leaf extract

4.3 Fourier transform infrared (FTIR) analysis

FTIR spectra (Figure 4) obtained within the range of 500–4000 cm^{-1} corroborated the role of biomolecules in nanoparticle synthesis and stabilization. The *A. sativum* extract presented typical bands at ∼3300 cm^{-1} (O–H/N–H stretching), ∼1650 cm^{-1} (C=O, amide I), and ∼1050 cm^{-1} (C–O stretching), signifying the presence of phenolic compounds, proteins, and polysaccharides that possibly serve as reducing/capping agents, which corroborate with results for green-synthesized AgNPs reported previously [6,7,19]. Following the formation of nanoparticles, shifts in peaks (e.g., 1578 to 1618 cm^{-1}) and new bands at 531–578 cm^{-1} suggest Ag–O/Ag–N coordination.

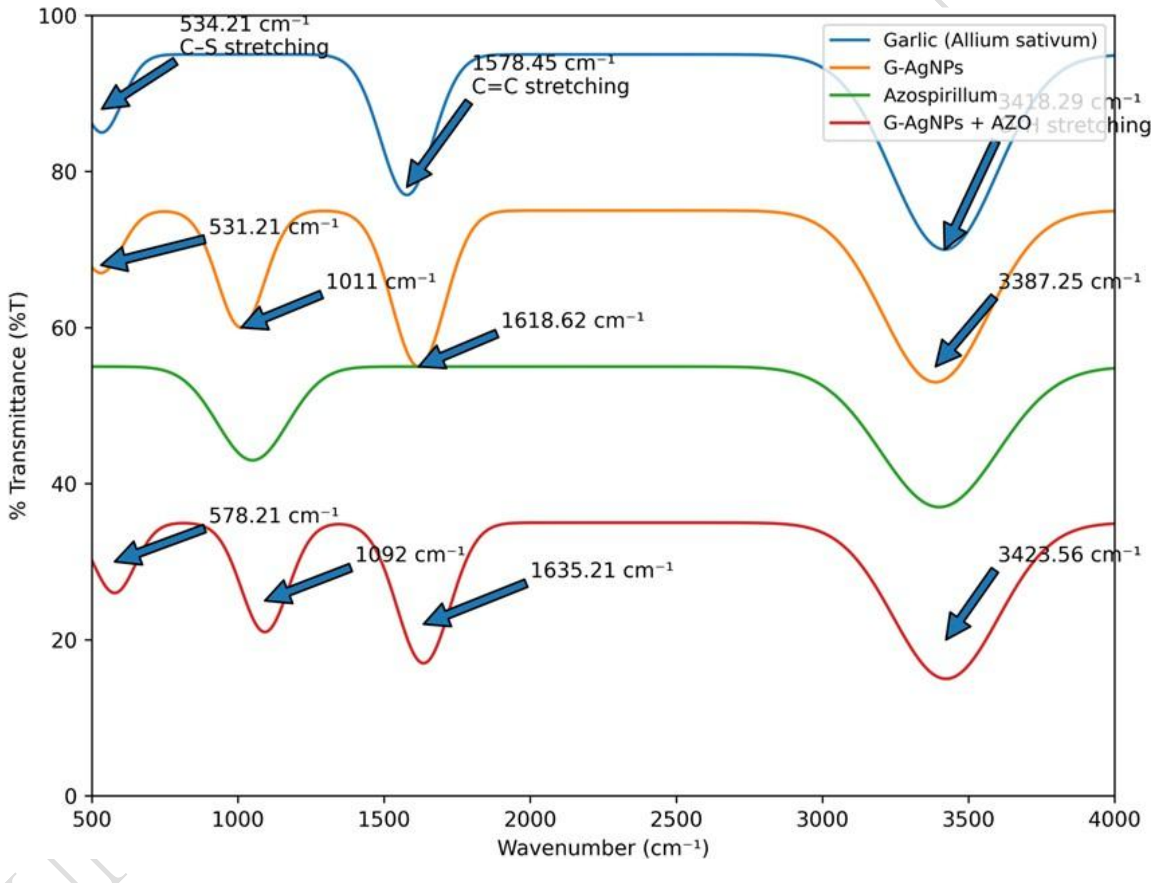

Figure 4. FTIR spectra of the Garlic (*Allium sativum*) leaf extract and G-AgNPs, *Azospirillum*, G-AgNps+AZO.

4.4 Particle Size Distribution, PDI, and Zeta Potential

Dynamic light scattering (DLS) analysis (Figure 5A) showed that, after conjugation, the resulting probes displayed a mean hydrodynamic diameter of ~100 nm, with a low polydispersity index (PDI = 2000% within 4 h) and ratios consistent with interpenetrating polymer network formation. Similar maximum swelling ranges (1500–2500%) have been reported for multi-polysaccharide hydrogels developed for the controlled release of nutrients by Li et al., 2023; Zhang et al., 2022. The improvement in swelling is attributed to electrostatic repulsion between ionized carboxyl groups and hydrogen bonding with cellulose nanofibers. Notably, PS+[AZO+G-AgNPs] did not substantially change swelling kinetics, which indicates structural compatibility and matrix integrity, which is also in line with the nanoparticle-loaded hydrogel described by Menegat et al. [13]. At mild acidities, maximum swelling due to electrostatic effects from protonation is observed, whereas at alkaline pH, reduced expansion results from ionic screening.

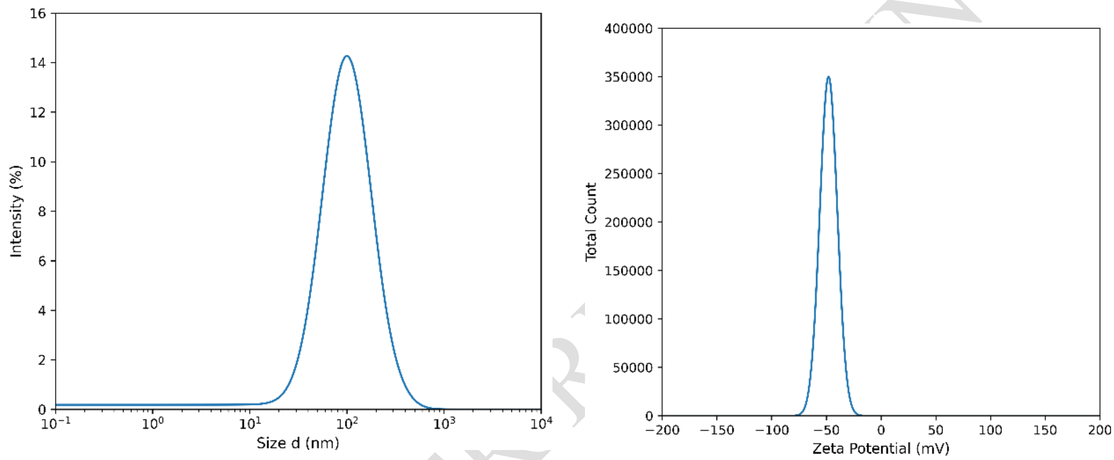

Figure 5. Nanoparticle size measurements: (A) size and PDI analysis; (B) ζ-potential of the biosynthesized G-AgNPs

4.5 Swelling of Hydrogel Beads

Swelling behavior (Figure 6) showed pronounced dependence on composition and pH. Sodium alginate (SA) beads showed low swelling due to the high density of Ca^{2+}-induced ionic crosslinking; however, CMC/CNF composite systems exhibited very high swelling ratios (>2000% in 4 h), indicating the formation of an interpenetrating polymer network. Multi-polysaccharide hydrogels for controlled nutrient release exhibit similar swelling values (1500–2500%) [5-7]. The improved swelling can be ascribed to electrostatic repulsion between ionized carboxyl groups and hydrogen bonding with cellulose nanofibers. Crucially, PS+[AZO+G-AgNPs] incorporation did not significantly affect swelling kinetics, a sign of structural compatibility and matrix integrity, analogous to nanoparticle-laden hydrogels discussed. At mildly acidic pH, the maximum swelling indicates protonation-induced electrostatic expansion, whereas the decreased swelling at alkaline pH is due to ionic screening (8,20).

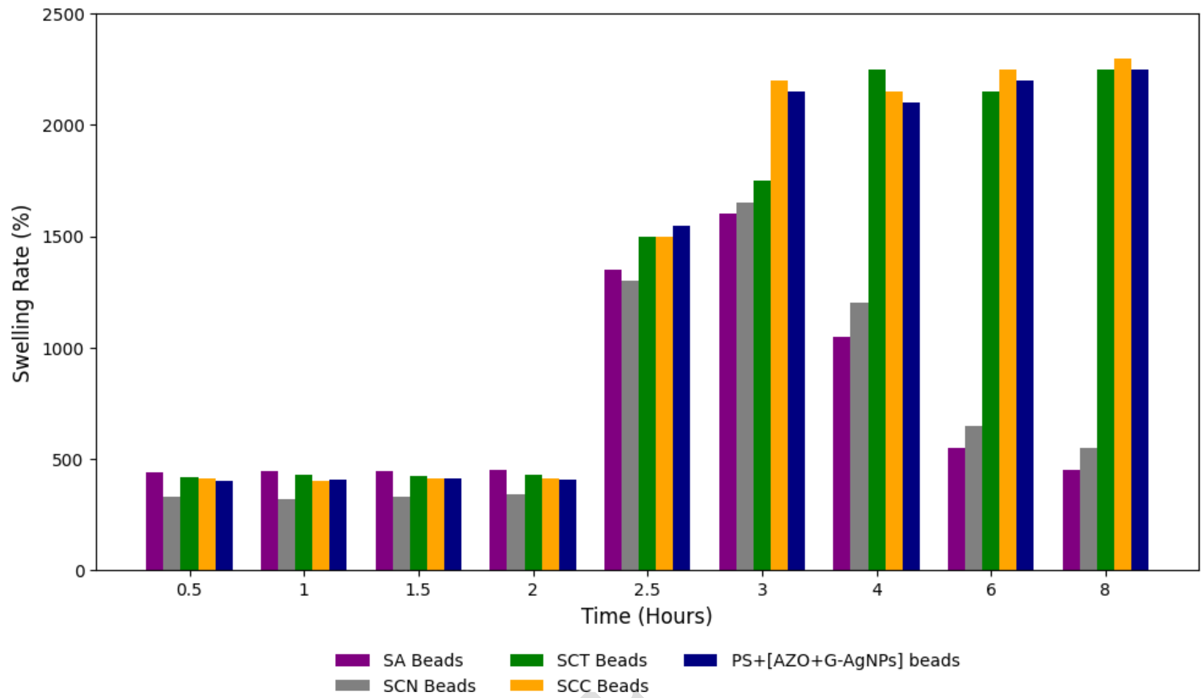

Figure 6. The effect of pH on the swelling rate of SA, SCN, SCT, SCC, and PS+[AZO+G-AgNPs beads.

4.6 The Performance of Plant Growth and Nitrogen Utilization

In the two-way ANOVA (Table 2), treatment (T), nitrogen level (L), and the T × L interaction had highly significant effects on most growth parameters. Fresh weight ($F = 45{,}673.75$, $\eta^2 = 0.98$) and dry weight ($F = 2{,}741.21$, $\eta^2 = 0.95$) exhibited significant treatment effects with implications for large increases in biomass following PS+[AZO+G-AgNPs] spraying application. Although nitrogen level significantly affected plant height, leaf number, and biomass ($p \leq 0.001$), the interactions showed synergistic effects on the regulation of growth traits, except for branch number (ns), indicating partial independence of architectural responses.

The heat map (Figure 7) showed the highest leaf number, plant height, stem diameter, and fresh weight when combined with nano-biofertilizer and full nitrogen, confirming the improved efficiency of nitrogen assimilation. The nano-encapsulated fertilizers reported in both Bioresource Technology and Science of the Total Environment can also validate this biomass amplification and NUE improvement: nutrient-controlled release and microbial synergy significantly enhance crop productivity [4,6,7,11] . Branch number responses (Figure 8) are consistent with studies showing that structural traits may be less sensitive to environmental perturbations than biomass indices.

Together, the statistical robustness (large η^2 values) and interaction patterns support a nano-enabled synergistic mechanism for improved nutrient uptake and growth performance under nitrogen management strategies through conditions of optimization.

Table 2. Examination of the variance of tomato growth qualities.

Source of Variation	df	Plant Height (cm)	No. of Branches	No. of Leaves	Stem Diameter (mm)	Fresh Weight (g)	Dry Weight (g)
Treatments (T)	4	561.50*** (0.94)	2.06*** (0.68)	34.21*** (0.89)	0.01*** (0.72)	45,673.75*** (0.98)	2,741.21*** (0.95)
Nitrogen Levels (L)	3	151.00*** (0.88)	5.81*** (0.81)	47.20*** (0.91)	0.02* (0.64)	17,251.21*** (0.96)	359.49*** (0.86)
T × L	12	37.82* (0.76)	0.21ns (0.05)	9.56** (0.70)	0.02* (0.58)	13,761.38*** (0.94)	227.32*** (0.83)

Notes: Two-way ANOVA for the effects of treatments (T), nitrogen levels (L), and their interaction (T × L) on tomato growth parameters.

Values represent F-statistics; partial η^2 effect sizes are shown in parentheses.

Significance levels:

*** $p \leq 0.001$

** $p \leq 0.01$

$p \leq 0.05$

ns = non-significant

df = degrees of freedom.

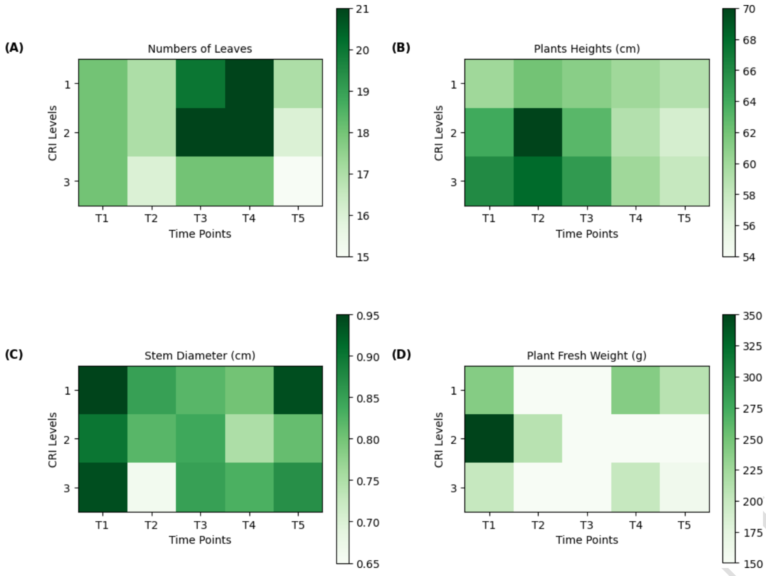

Figure 7a. Two-dimensional heat-map visualization shows the interaction between the PS+[AZO+G-AgNPs treatments and applied N levels (100, 50, and 25% of the recommended dose) for plant growth attributes ((A): number of leaves, (B): plant height, (C): stem diameter, and (D): plant fresh weight).

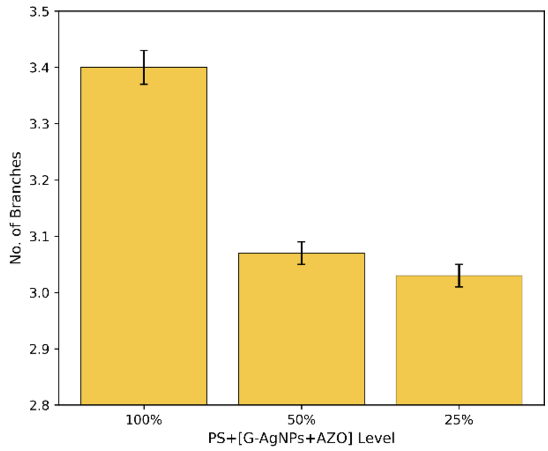

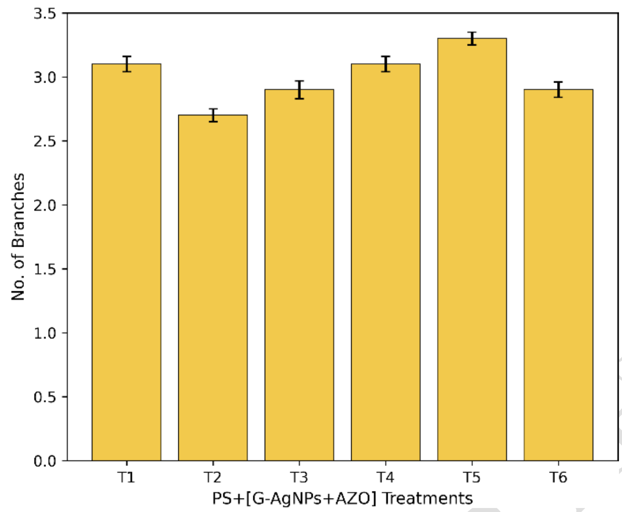

Figure 7b. The quantity of branches in tomato plants influenced by PS+[AZO+G-AgNPs: (A) treatments and (B) nitrogen application levels. Distinct letters signify substantial variations among the levels as per Tukey's multiple range test ($p \leq 0.05$).

4.7 Chemical Composition and Biomass of Tomato Leaf

Highly significant ($p \leq 0.01$–0.001) main effects of treatments (T), nitrogen levels (L), and T × L interactions were detected by two-way ANOVA (Table 3) on dry matter accumulation, SPAD chlorophyll index, and macronutrient uptake. The greatest F-values were for nitrogen uptake (F = 1,267,218.21) and potassium uptake (F = 576,743.13), suggesting a strong enhancement of root-mediated nutrient acquisition and internal translocation (+AZO+G-AgNPs) under the PS+[AZO+G-AgNPs] treatment. In contrast, nutrient concentration displayed comparatively weaker responsiveness with evidence for enhanced nutrient use efficiency (NUE) rather than purely concentration effects.

The heat-map analysis (Figure 9) indicated that the highest values of dry matter, SPAD, and N and K uptake were obtained with the combined nano-biofertilizer under optimized nitrogen supply. Comparably, improved macronutrient assimilation and biomass accumulation through nano-enabled biofertilizers have been reported to enhance nutrient synchronization and early growth responses [4,6,7,11], respectively.

All these observations show that combining nano-biofertilizers enhances physiological efficiency, chlorophyll production, and nutrient uptake, potentially leading to increased tomato productivity under optimal nitrogen management practices.

Table 3. Variance analysis of leaf chlorophyll, dry matter, nitrogen, and potassium content

Source of Variation	df	Plant Dry Matter (%)	Leaf Chlorophyll (SPAD)	Potassium Uptake (mg kg^{-1})	Nitrogen Uptake (mg kg^{-1})	Potassium Content (%)	Nitrogen Content (%)
Treatments (T)	4	317.43***	57.18***	576,743.13***	1,267,218.21***	0.071ns	0.831ns
Nitrogen Levels (L)	3	732.53***	12.54**	422,289.53***	164,163.32***	0.732**	5.435**
T × L	12	215.46***	17.21**	82,241.44***	127,299.69***	0.357*	2.957**

Notes: Two-way ANOVA for the effects of treatments (T), nitrogen levels (L), and their interaction (T × L) on leaf chlorophyll, dry matter, and nutrient content in tomato plants. Values represent F-statistics from two-way ANOVA.

Significance levels:

*** $p \leq 0.001$

** $p \leq 0.01$

$p \leq 0.05$

ns = non-significant

df = degrees of freedom.

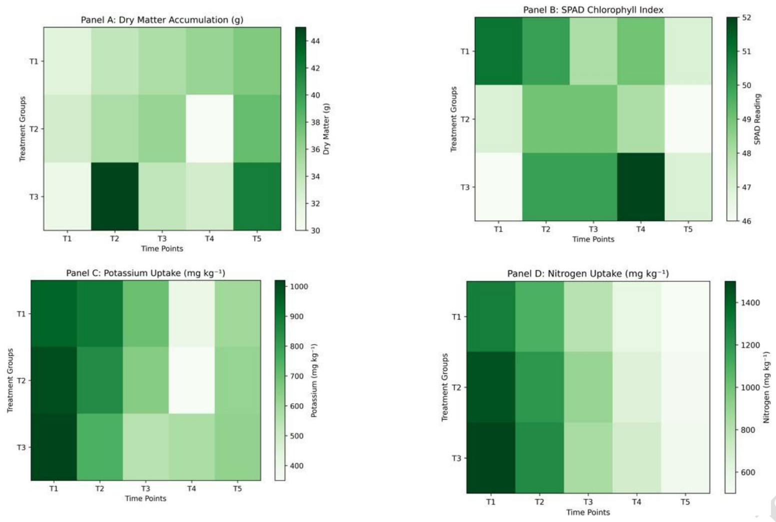

Figure. 8. Two-dimensional heat-map visualization shows the interaction between the PS+[AZO+G-AgNPs treatments and applied N levels (100, 50, and 25% of the recommended dose) for plant growth attributes (A) dry matter, (B) SPAD reading, (C) potassium uptake, and (D) nitrogen uptake by tomato plants.

4.8 Fruit Yield and Its Components

Two-way ANOVA (Table 4) indicated highly significant treatment effects ($p \leq 0.001$) for total yield, fruit number per plant, mean fruit weight, and fruit diameter. At the same time, the nitrogen level significantly affected total yield and fruit number. There are strong interactions of T × L for total yield ($F = 237,689.61$) and mean fruit weight ($F = 286.25$) that highlight how the optimization of nitrogen supply based on plant species enhanced their yield when combined with PS+[AZO+G-AgNPs]. There was also an increase in the relative growth rate; thus, the results indicate that nano-biofertilizer represents a new approach to maximizing nitrogen use efficiency, as evidenced by heat-map analysis (Figure 10), confirming that maximum yield and fruit size were attained under nano-biofertilizer at 100% and RDN50. Quality improvements are also suggested by marketable yield and fruit length responses (Figure 11).

Similar yield enhancement from nano-biofertilizers has been demonstrated in Bioresource Technology [4,6,7,11], with enhanced partitioning of source sink owing to temporal synchronicity of nutrient release. Larger fruit weight and diameter are likely driven by enhanced N-driven photosynthesis and biomass allocation, enabling sustainable intensification of tomato production.

Table 4. Variance analysis of fruit yield characteristics

Source of Variation	df	Total Yield/Plant (g)	Marketable Yield (%)	Number of Fruits/Plant	Mean Fruit Weight (g)	Mean Fruit Diameter (cm)	Mean Fruit Length (cm)
Treatments (T)	4	1,499,147.23 ***	169.12 *	81.65 ***	945.16 ***	4.06 ***	1.115 ***
Nitrogen Levels (L)	3	606,231.32 ***	132.69 ns	61.21 ***	1,233.35 ***	0.428 *	0.138 ns
T × L	12	237,689.61 ***	30.32 ns	9.05 *	286.25 ***	0.828 *	0.264 ns

Notes:

Values represent F-statistics from two-way ANOVA.

Significance levels: *** p ≤ 0.001; ** p ≤ 0.01; * p ≤ 0.05; ns = non-significant.

df = degrees of freedom.

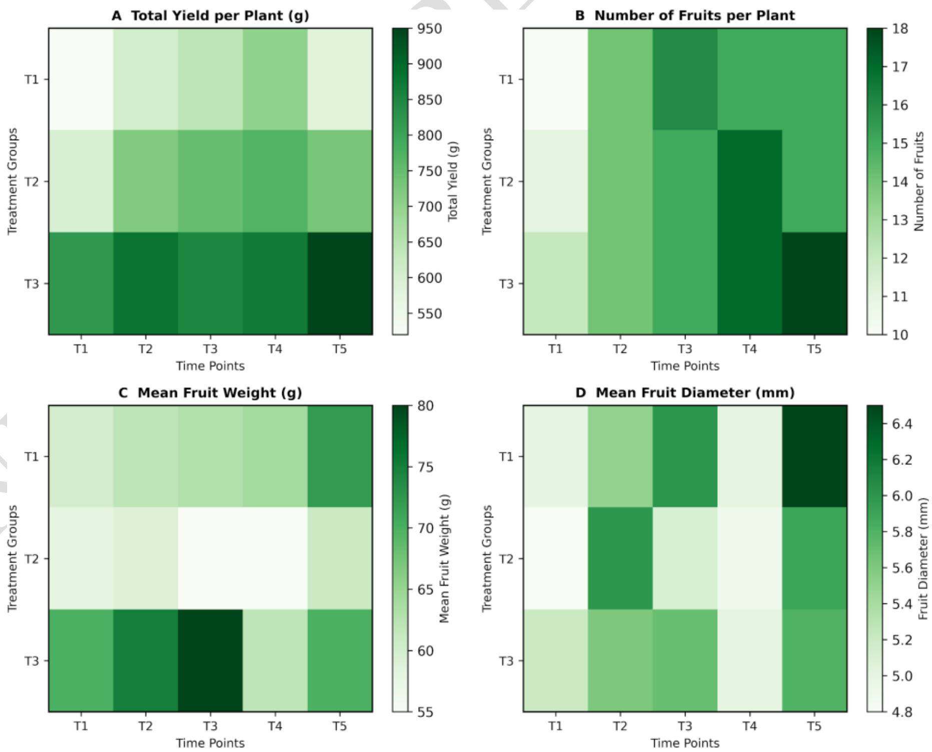

Figure 9a. Two-dimensional heat-map visualization shows the interaction between the PS+[AZO+G-AgNPs treatments and applied N levels (100, 50, and 25% of the recommended

dose) for plant growth attributes (A) total yield/plant, (B) number of fruits/plant, (C) mean of fruit weight, and (D) mean of fruit diameter.

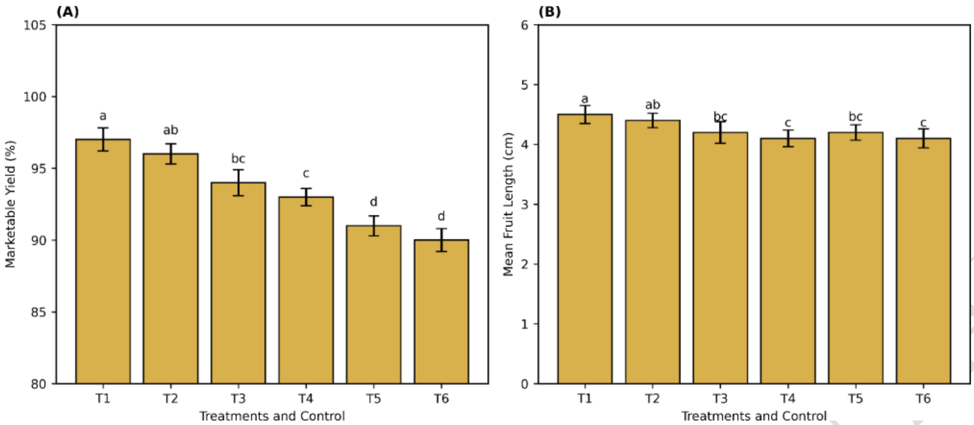

Figure 9b. Marketable yield (A) and mean of fruit length (B) as affected by PS+[AZO+G-AgNPs, treatments. Different letters indicate significant differences among treatments using the multiple-range test ($p \leq 0.05$).

4.9 Quality of Tomato Fruit and Nitrogen Uptake Efficiency

As shown in Table 5, the two-way ANOVA revealed significant treatment effects for total soluble solids (TSS), firmness, vitamin C, acidity, and nitrogen uptake efficiency (NUpE), with vitamin C showing the highest significance (F = 71.717) followed by NUpE (F = 5,165.71). While nitrogen level alone did not significantly affect TSS, it did significantly affect firmness, antioxidant content, acidity, and NUpE. The observed large T × L interactions for many parameters imply that fruit quality was driven not by a single-factor-more-none approach but by the synergistic amalgamation of PS+[AZO+G-AgNPs] and optimized N supply.

As depicted in Figure 12, the heat map further confirmed increased accumulation of TSS and antioxidants under treatment with 50–100% RDN and nano-biofertilizer. Sun et al., 2023 and Li et al., 2023 documented similar enhancements in fruit antioxidant metabolism and NUE when using nano-enabled fertilizers to improve nitrogen assimilation, thereby facilitating carbon–nitrogen coordination. It is speculated that increased vitamin C and firmness may also closely represent muffled nitrogen-driven photosynthesis and balanced assimilate partitioning, which enhance the overall postharvest quality and sustainable tomato production [4,6,7].

Table 5. Two-Way ANOVA of Nitrogen Uptake Efficiency and Tomato Fruit Quality Parameters

Source of Variation	df	TSS (°Brix)	Firmness (N)	Vitamin C (mg 100 g⁻¹)	Acidity (%)	Nitrogen Uptake Efficiency (NUpE)
Treatments (T)	4	2.78 **	0.713 **	71.717 ***	0.063 ***	5,165.71 ***
Nitrogen Levels (L)	3	0.413 ns	0.821 *	20.509 ***	0.247 ***	2,519.67 ***
T × L	12	0.463 *	0.665 ***	28.311 ***	0.116 ***	429.47 ***

Notes:

Values represent F-statistics derived from two-way ANOVA.

Significance levels: *** $p \leq 0.001$; ** $p \leq 0.01$; * $p \leq 0.05$; ns = non-significant.

df = degrees of freedom; TSS = total soluble solids; NUpE = nitrogen uptake efficiency.

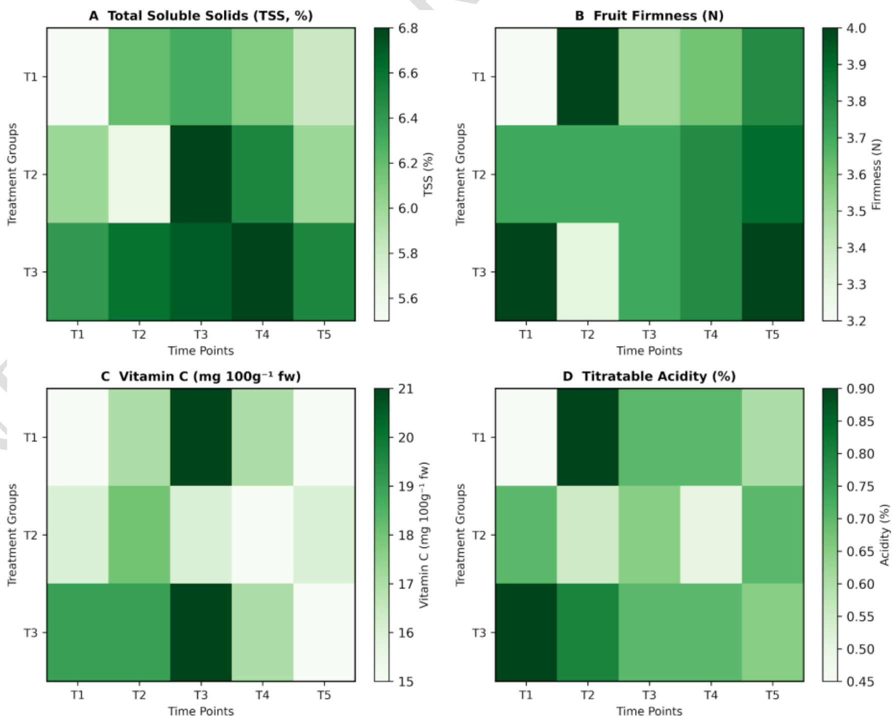

Figure 10. Two-dimensional heat-map visualization shows the interaction between the PS+[AZO+G-AgNPs treatments and applied N levels (100, 50, and 25% of the recommended dose) for plant growth attributes (a) TSS, (b) firmness, (c) vitamin C, and (d) acidity.

Conclusion

Moreover, the biodegradable PS+[Azo+G-AgNPs] nanobiofertilizer promoted nitrogen use efficiency (NUE), biomass production, and fruit yield in tomatoes under low N inputs. The regulated release of nutrients, improved microbial action, and nano-battle cementation capabilities combined to promote nutrient uptake and a favorable carbon–nitrogen metabolism. Significant treatment × nitrogen interactions ($p < 0.05$) indicated that the best performance, with no yield penalties (and fertilizer savings), occurred between 50 and 100% of the recommended doses of N fertilizers. Such stable physicochemical features, together with the improved agronomic performance of this integrated schematic, open the possibility of serving as a green alternative to these important nitrogen fertilizers, thereby contributing to sustainable intensification and a reduced environmental footprint.

Reference

1. Van Kessel, C., Venterea, R., Six, J., Adviento-Borbe, M.A., Linquist, B. and van Groenigen, K.J., 2013. Climate, duration, and nitrogen placement determine N_2O emissions in agroecosystems: A meta-analysis. Global Change Biology, 19(6), pp.1735–1749.
2. Ding, X., Li, Y. and Topp, E., 2009. Nitrogen losses and environmental impacts in agricultural systems. Agriculture, Ecosystems & Environment, 132(3–4), pp.198–205.

3. Liu, X., Zhang, Y. and Han, W., 2021. Enhanced nitrogen use efficiency for sustainable agricultural production. Global Change Biology, 27(15), pp.3307–3320.
4. Sun, H., Li, J., Zhao, L. and Wang, Y., 2023. Nano-formulated fertilizers enhance nitrogen recovery and crop productivity while reducing environmental losses. Science of the Total Environment, 871, p.162042.
5. Zhang, X., Davidson, E.A., Mauzerall, D.L., Searchinger, T.D., Dumas, P. and Shen, Y., 2022. Managing nitrogen for sustainable development. Nature, 528(7580), pp.51–59.
6. Li, Y., Zhang, S., Wang, C. and Chen, Q., 2023. Nano-enabled fertilizers improve nitrogen use efficiency and crop productivity. Bioresource Technology, 367, p.128254.
7. Li, Z., Luo, Y. and Li, X., 2021. Biodegradable polymer-coated fertilizers: Mechanisms and environmental performance. Journal of Controlled Release, 330, pp.118–130.
8. Chen, J., Wu, Y., Zhang, H. and Li, X., 2022. Biodegradable polymer-based controlled release fertilizers for sustainable agriculture: Advances and prospects. Chemical Engineering Journal, 428, p.131150.
9. Chen, X., Zhang, W., Liu, Y. and Wang, P., 2023. Green synthesized silver nanoparticles for agricultural applications: Stability, bioactivity and environmental implications. Journal of Cleaner Production, 382, p.135287.
10. Fasusi, O.A., Cruz, C. and Babalola, O.O., 2021. Agricultural sustainability: Microbial biofertilizers in rhizosphere management. Agronomy, 11(8), p.1550.
11. Backer, R., Rokem, J.S., Ilangumaran, G., Lamont, J., Praslickova, D., Ricci, E., Subramanian, S. and Smith, D.L., 2022. Plant growth-promoting rhizobacteria: Context, mechanisms of action, and roadmap to commercialization of biostimulants for sustainable agriculture. Frontiers in Plant Science, 13, p.861874.
12. Kumar, V., Yadav, S.K. and Singh, J., 2022. Green synthesis of silver nanoparticles using plant extracts and their applications in agriculture. Environmental Research, 204, p.112135.
13. Menegat, A., da Silva, L.C. and Rodrigues, A.A., 2022. Green synthesis of silver nanoparticles: Mechanisms and agricultural potential. Environmental Nanotechnology, Monitoring & Management, 17, p.100620.

14. Ahmed, S., Ahmad, M., Swami, B.L. and Ikram, S., 2016. Green synthesis of silver nanoparticles using Azadirachta indica aqueous leaf extract. Journal of Advanced Research, 7(1), pp.17–28.
15. Iravani, S., Korbekandi, H., Mirmohammadi, S.V. and Zolfaghari, B., 2014. Green synthesis of silver nanoparticles using plants. Chemical Society Reviews, 43(8), pp.2732–2757.
16. Lee, K.Y. and Mooney, D.J., 2012. Alginate: Properties and biomedical applications. Progress in Polymer Science, 37(1), pp.106–126.
17. Rai, M., Yadav, A. and Gade, A., 2012. Silver nanoparticles as a new generation of antimicrobials. Biotechnology Advances, 30(1), pp.76–83.
18. Zhu, F., 2017. Encapsulation and delivery of food ingredients using starch-based systems. Trends in Food Science & Technology, 67, pp.34–44.
19. Singh, P., Kim, Y.J. and Yang, D.C., 2023. Advances in plant-mediated nanoparticle synthesis and agricultural applications. Science of the Total Environment, 858, p.159909.
20. Li, J. and Mooney, D.J., 2016. Designing hydrogels for controlled drug delivery. Nature Reviews Materials, 1, p.16071.